Composites Part B 167 (2019) 250–262

Contents lists available at ScienceDirect

Composites Part B

journal homepage: www.elsevier.com/locate/compositesb

Enhanced simple beam theory for characterising mode-I fracture resistance via a double cantilever beam test

Leo Škec[a,*], Giulio Alfano[a], Gordan Jelenić[b]

[a] Department of Mechanical and Aerospace Engineering, Brunel University London, Kingston Lane, Uxbridge, UB8 3PH, UK
[b] Faculty of Civil Engineering, University of Rijeka, Radmile Matejčić 3, 51000, Rijeka, Croatia

ARTICLE INFO

Keywords:
DCB test
Mode I delamination
Analytical solution
Timoshenko beam theory
Linear-elastic fracture mechanics
Data-reduction schemes

ABSTRACT

We study a double-cantilever beam (DCB), in which either the crack-mouth opening displacement or the end rotations are prescribed, in the linear-elastic-fracture-mechanics (LEFM) limit of an infinitely stiff and brittle interface. We present a novel, yet extremely simple, derivation of the closed-form solution of this problem when the arms are modelled with Timoshenko beam theory. We remove the assumption that the cross sections of the DCB arms are assumed not to rotate (i.e. that they are clamped) at the crack tip, which is made in so-called 'simple beam theory' (SBT). Therefore, with our 'enhanced simple beam theory' (ESBT), in front of the crack tip, cross sections are allowed to rotate, although the beam axis stays undeformed. Thus, we can determine the crack-tip rotation caused by the deformation of the beam in front of the crack tip also in the LEFM limit. As a result, most of the inaccuracies of the SBT are eliminated, without the need for a crack-length correction, used in the 'corrected beam theory' (CBT). In this way, we can derive a very accurate data reduction formula for the critical energy release rate, G_c, which does not require the measurement of the crack length, unlike CBT. In our numerical results we show that, compared to the most effective data reduction methods currently available (including CBT), our formula is either as accurate or more accurate for the case of brittle delamination of thick composite plates, in which shear deformability can play a significant role.

1. Introduction

Determining the fracture resistance of adhesives or laminated composites is nowadays essential for their industrial application. Standardised procedures have been developed for different types of specimens and modes of delamination (debonding). Such procedures are based on relatively simple tests used to produce data which are then processed using one of several data reduction schemes proposed. Thus, we can say that standards for determining the fracture resistance of adhesives consist of two main parts: (i) the experimental part (where details on how to prepare and perform the experiments are given) and (ii) the post-processing part (where expressions for computing the fracture resistance from the experimental data are contained). In this work we will concentrate only on the second (post-processing) aspect for the standard double cantilever beam (DCB) test used for determining the fracture resistance in mode I.

Based on the work of Ripling and his co-workers in the mid 1960s and early 1970s [1], a first ASTM standard for determining fracture resistance of adhesives in mode I was released. Up to the present day, this standard has not changed considerably and its current version, ASTM D3433-99(2012) [2], still uses the same expressions for the fracture resistance that Ripling et al. proposed in Ref. [1]. The original standard, which introduced the DCB specimen, used the critical energy release rate, G_c, as the measure of fracture resistance of the adhesive. Expressions for G_c were derived from linear elastic fracture mechanics (LEFM) theory under the assumptions that the DCB arms act as if they were Timoshenko beams clamped at the crack tip and the interface material is infinitely stiff and perfectly brittle. We will refer to such models as 'simple beam theory' (SBT) models. In fact, the same formula proposed by Ripling et al. [1] and used in ASTM D3433-99(2012) [2] is also used in the British Standard BS ISO 25217:2009 [3] under the name 'simple beam theory' (SBT).

However, Ripling himself [1] noticed that this simple model of the real problem, under a given load, resulted in deflections smaller than the ones obtained from the actual experiments. He attributed this to the fact that the arms of the DCB, rather than being clamped, actually rotate at the crack tip. Furthermore, he suggested that the expression for G_c derived under the assumption that the arms are clamped at the crack tip could be corrected by adding some extra length to the actual crack length. Following the same line of reasoning, so-called 'corrected beam

* Corresponding author.
E-mail addresses: leo.skec@brunel.ac.uk, leo.skec@uniri.hr (L. Škec), giulio.alfano@brunel.ac.uk (G. Alfano), gordan.jelenic@uniri.hr (G. Jelenić).

https://doi.org/10.1016/j.compositesb.2018.11.099
Received 11 May 2018; Received in revised form 17 September 2018; Accepted 25 November 2018
Available online 07 December 2018

theory' (CBT) was introduced in the British Standard [3] and it is considered as one of the most accurate data reduction schemes currently available in the standards [4–6].

In this work we revisit the SBT assumption that the arms are clamped at the crack tip. Even if in reality the arms were connected by an infinitely rigid and perfectly brittle interface, it is expected that they would deform around the crack tip. This behaviour could be captured using 3D or 2D solid finite element models, but it can be also captured if the arms are modelled as Timoshenko beams, which is less obvious. It the latter case, although transverse separation at the interface is not allowed, the arms rotations due to shear still are. Consequently, the arms of a DCB will act as clamped only if they are shear-rigid, which corresponds to Euler-Bernoulli beam theory. The rotation of the arms at and in front of the crack tip is something that, to the best of authors' knowledge, has not been included so far in approaches that combine Timoshenko beam theory and LEFM. Thus, we will call our approach 'enhanced simple beam theory' (ESBT). As already mentioned, when Euler-Bernoulli beam theory is used, ESBT is equivalent to SBT.

Based on our ESBT solution, we derive a novel expression for G_c that accounts for the rotation at the crack tip. Using the so-called 'equivalent crack length' approach [6,7], we derive a data reduction scheme based on the ESBT model that does not require the measurement of the crack length and is therefore practical and, as confirmed by our numerical results, very accurate. Measuring the crack length is, in fact, common in all the available data reduction schemes in the current versions of American and British Standards for determining fracture resistance in modeI [2–4]. This is usually performed using a travelling microscope or a high-resolution camera, which can be time-consuming and prone to inaccuracy. Thus, following our work from Ref. [6], in this work we dedicate special attention to data reduction schemes that do not require the measurement of the crack length.

Beside the novel ESBT data reduction scheme, in this work we consider Euler-Bernoulli and Timoshenko versions of SBT data reduction schemes that do not require the measurement of the crack length and are already known from the literature [7–9]. Based on virtual experiments, where numerical models are used to create input data for data-reduction schemes, we compare the data-reduction schemes that do not require measurement of the crack length (including ESBT) with those available in BS-ISO 25217:2009 [3] standard. The accuracy of each data reduction scheme is assessed by how close the computed value of G_c matches the input value of the work of separation (area under the traction-separation law) of the cohesive-zone model (CZM) used at the interface in the numerical analysis.

The structure of the paper is as follows. In Section 2, we define the problem and derive the closed-form solutions in terms of contact tractions at the interface, bending moments, shear forces and cross-sectional rotations of the upper arm. In Section 3, we derive expressions for the cross-head displacement and the critical energy release rate. One data-reduction scheme based on ESBT and two other ones (Euler-Bernoulli and Timoshenko) based on SBT are derived in Section 4. They all use the concept of equivalent crack length and, therefore, do not require measurement of the crack length. In Section 5, we assess the accuracy of these data-reduction schemes and compare it to that provided by the of formulae provided in BS ISO 25217:2009 [3]. In Section 6 we summarise the main contributions of the paper and give some recommendations for future work. The solution of the problem of a DCB with prescribed rotations based on ESBT assumptions and the corresponding formula for G_c are given in Appendix A.

2. Definition and solution of the problem

2.1. Problem description

We consider a double cantilever beam (DCB) composed of two identical arms with length L, arm depth h and width b as shown in Fig. 1. At the left-hand side there is an initial notch of length a_0 between the arms, whereas on the rest of the interface the arms are connected. At the left-hand end, the bottom arm is pinned, whereas on the upper arm a transversal displacement δ is applied. As a consequence, two identical, but opposite transverse forces F act on the arms at the left-hand end. Because these forces are applied symmetrically with respect to the mid-plane of the interface between the two arms, stresses and strains in the arms are symmetrical with respect to the mid-plane of the interface, too. Thus, for the sake of simplicity, only one arm of the DCB can be considered in the analysis. In particular we will consider only the upper arm and assume that the x-axis is the centroidal axis of the arm (reference axis), while y and z axes are the principal axes of the arm's cross section.

We model the arm as a Timoshenko beam with linear-elastic constitutive law, where material properties are defined by Young's modulus, E, and shear modulus, μ. In a general case E and μ can have independent values, while for an isotropic material $\mu = 0.5E/(1+\nu)$, where ν is Poisson's ratio. We denote the bending stiffness of the upper arm by EI, where $I = bh^3/12$ is the second moment of area, and the shear stiffness by μA_s where $A_s = A\,k_s$ is the shear-corrected cross-sectional area with $A = bh$ and $k_s = 5/6$. The use of Timoshenko beam theory also implies that we assume that displacements and rotations of the arms are relatively small compared to the specimen's dimensions.

We assume that the interface connection between the arms is infinitely stiff and perfectly brittle, which means that there is no separation at a point of the interface before the crack reaches that point. Such a model corresponds to LEFM, where it is assumed that the crack will propagate when a critical value of the energy release rate, G_c, is reached. In the following section we will derive a closed-form expression for G_c for a DCB with arms modelled as Timoshenko beams and an infinitely stiff, perfectly brittle interface.

2.2. Solution of the differential equations of the problem

According to Fig. 1, the x-axis corresponds to the centroidal line of the upper arm, whereas the y-axis passes through the crack tip, i.e. between the cracked and undamaged part of the DCB. We will focus on the undamaged part and investigate what happens in front of the crack tip.

The general form of the differential equation for a Timoshenko beam with constant bending and shear stiffness reads

$$\upsilon^{\mathrm{IV}}(x) - \frac{1}{EI}q(x) + \frac{1}{\mu A_s}q''(x) = 0, \tag{1}$$

where υ is the transversal displacement of the upper arm in y-direction and q is the distributed load on the arm which is positive when pointing upwards. Because for an infinitely stiff interface in front of the crack tip $\upsilon(x) = 0$, and thus $\upsilon^{\mathrm{IV}}(x) = 0$, Equation (1) becomes

$$q''(x) - \alpha\, q(x) = 0, \quad \text{for} \quad x > 0, \tag{2}$$

where $\alpha = \mu A_s/EI$. Note also that the contact tractions on the interface can be defined as

$$\sigma(x) = -\frac{q(x)}{b}. \tag{3}$$

The solution of Equation (2) is

$$q(x) = e^{\sqrt{\alpha}x}c_1 + e^{-\sqrt{\alpha}x}c_2, \quad \text{for} \quad x > 0, \tag{4}$$

where c_1 and c_2 are integration constants.

Remark 2.1. It can be easily shown that solution (4) is a particular case of the solution of a Timoshenko beam on a Winkler foundation. Assuming linear-elastic springs defined by the stiffness k in N/mm^3, it follows that $\upsilon(x) = -q(x)/(2\,k)$. Thus, for the particular case when $k \to \infty$, the first member in Equation (1) vanishes, i.e. $\upsilon^{\mathrm{IV}}(x) = 0$. Solutions for a beam on a Winkler foundation for finite values of k are available in the literature [10–12]. ■

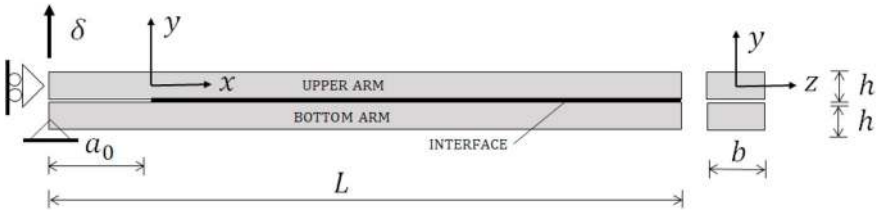

Fig. 1. Geometry of a DCB specimen.

The following beam theory relations

$$q(x) = \mathscr{T}'(x), \tag{5}$$

$$\mathscr{T}(x) = \mathscr{M}'(x), \tag{6}$$

$$\mathscr{M}(x) = EI\varphi'(x), \tag{7}$$

where $\mathscr{T}$ and $\mathscr{M}$ are the shear force and the bending moment in the upper arm, respectively, and $\varphi(x)$ is the arm's cross-sectional rotation defined as

$$\varphi(x) = \upsilon'(x) + \frac{\mathscr{T}(x)}{\mu A_s}, \tag{8}$$

give us

$$\mathscr{M}(x) = \frac{q(x)}{\alpha}, \quad \text{for} \quad x > 0. \tag{9}$$

because, again, $\upsilon'(x) = 0$ for $x > 0$.

We assume the crack is sufficiently distant from the free (right-hand side) end of the specimen, in a way that all the boundary effects on the right-hand end of the specimen can be neglected. Thus, we can assume an infinite length of the arm and write the following conditions

$$\lim_{x\to\infty} \varphi(x) = \lim_{x\to\infty} \mathscr{T}(x) = \lim_{x\to\infty} \mathscr{M}(x) = 0. \tag{10}$$

This condition and Equation (9) give

$$\lim_{x\to\infty} q(x) = 0, \tag{11}$$

from which it follows that $c_1 = 0$. The remaining constant is determined for any position of the crack, a, from the equilibrium of moments about the crack tip as

$$F\,a - c_2 \int_0^\infty e^{-\sqrt{\alpha}x} x \; \mathrm{d}x = 0. \tag{12}$$

Hence, after integrating by parts, we obtain

$$c_2 = F\,a\,\alpha. \tag{13}$$

Finally, in front of the crack tip ($x > 0$) we have

$$q(x) = F\,a\,\alpha\, e^{-\sqrt{\alpha}x}, \tag{14}$$

and from Equations (3), (6), (8) and (9), respectively, we obtain

$$\sigma(x) = \frac{-F\,a\,\alpha}{b} e^{-\sqrt{\alpha}x}, \tag{15}$$

$$\mathscr{M}(x) = F\,a\,e^{-\sqrt{\alpha}x}, \tag{16}$$

$$\mathscr{T}(x) = -F\,a\,\sqrt{\alpha}\,e^{-\sqrt{\alpha}x}, \tag{17}$$

$$\varphi(x) = -\frac{F\,a}{EI\,\sqrt{\alpha}} e^{-\sqrt{\alpha}x}. \tag{18}$$

Although these functions have only been obtained for $x > 0$, we can notice that

$$\lim_{x\to 0^+} \mathscr{M}(x) = F\,a, \tag{19}$$

$$\lim_{x\to 0^+} \mathscr{T}(x) = -F\,a\,\sqrt{\alpha}. \tag{20}$$

On the other hand, from the part of the DCB where the arms are detached, we know that the bending moments in the upper arm vary linearly and the shear forces are constant, i.e. for $-a \le x < 0$ we have

$$\mathscr{M}(x) = F(x + a), \tag{21}$$

$$\mathscr{T}(x) = F. \tag{22}$$

It follows that

$$\mathscr{M}(0) = \lim_{x\to 0^-} \mathscr{M}(x) = \lim_{x\to 0^+} \mathscr{M}(x) = F\,a, \tag{23}$$

$$\lim_{x\to 0^-} \mathscr{T}(x) = F. \tag{24}$$

By comparing Equations (16), (19) and (23), and Equations (20) and (24), we can notice that, at the crack tip ($x = 0$), there is a cusp in the function of bending moments and a discontinuity in the function of shear forces (as shown in Fig. 2). This implies that, at the crack tip, there must be a concentrated transversal force. This force, denoted by F_0, is responsible for the jump in the function of shear forces from the value F to the value $-Fa\sqrt{\alpha}$, which means that it is pointing downwards and its value is

$$F_0 = F(1 + a\sqrt{\alpha}). \tag{25}$$

Thus, by taking into account the entire domain ($x \ge -a$), we can write

$$\mathscr{T}(x) = \begin{cases} F & \text{for } -a \le x < 0, \\ -F\,a\,\sqrt{\alpha}\,e^{-\sqrt{\alpha}x} & \text{for } x > 0, \end{cases} \tag{26}$$

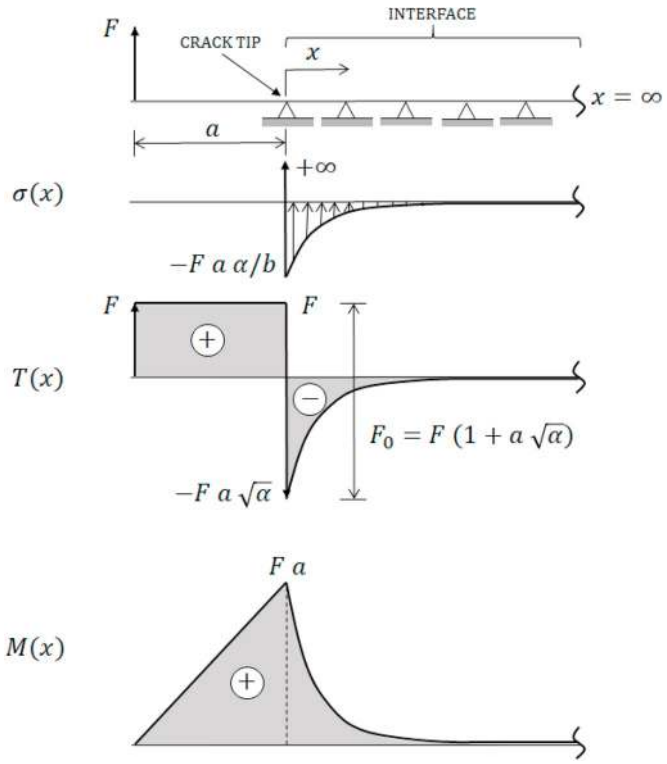

Fig. 2. Diagrams of contact tractions, $\sigma(x)$, shear forces, $\mathscr{T}(x)$, and bending moments, $\mathscr{M}(x)$, in the upper arm of a DCB with prescribed displacement.

$$\mathscr{M}(x) = \begin{cases} F(x+a) & \text{for } -a \le x \le 0, \\ F\ a\ e^{-\sqrt{\alpha}x} & \text{for } x \ge 0, \end{cases} \tag{27}$$

Also, by taking into account (5), we can define

$$q(x) = \begin{cases} 0 & \text{for } -a \le x < 0, \\ F\ a\ \alpha\ e^{-\sqrt{\alpha}x} & \text{for } x > 0, \end{cases} \tag{28}$$

which, according to (3), gives

$$\sigma(x) = \begin{cases} 0 & \text{for } -a \le x < 0, \\ -\frac{F\ a\ \alpha}{b} e^{-\sqrt{\alpha}x} & \text{for } x > 0. \end{cases} \tag{29}$$

As expected, on the detached part of the DCB ($-a \le x < 0$) there are no contact tractions, but on the interface between the arms ($x > 0$) there are compressive tractions (σ and q are pointing upwards). Because the resultant of these tractions, as well as the applied load on the upper layer, F, is pointing upwards, to obtain the equilibrium of transversal forces there must exist another concentrated force pointing downwards. We already showed that this reaction force, defined as F_0 in (25), is acting at the crack tip.

This result means that, at the crack tip, Timoshenko beam theory predicts an infinite positive (i.e. tensile) value of the interface stress orthogonal to the crack (see Fig. 2). Note also that $\sigma(x)$ is not defined for $x = 0$ in (29). However, unlike the stress singularity found in LEFM using continuum models, Timoshenko beam theory also predicts that the tensile-stress zone in front of the crack tip shrinks to a point (and so does also Euler-Bernoulli beam theory), which effectively means that the tensile stress profile becomes a Dirac delta function. This is clearly a result of the assumption, made in the beam theories, that beam cross sections do not deform within their plane.

We will express the cross-sectional rotations of the upper arm using Equation (7) to obtain

$$\varphi(x) = \int \mathscr{M}(x)\mathrm{d}x/EI + c_3, \tag{30}$$

where c_3 is an integration constant. Note that $\mathscr{M}(x)$, according to (27), is defined differently for $-a \le x \le 0$ and for $x \ge 0$. For $x \ge 0$, from the boundary condition $\varphi(\infty) = 0$ we obtain $c_3 = 0$. Furthermore, because $\mathscr{M}(x)$ has C^0 continuity, $\varphi(x)$ has C^1 continuity over the entire domain ($x \ge -a$). This means that at the crack tip, using solution (18) for $\varphi(x)$ valid for $x > 0$, we can write

$$\varphi(0) = \lim_{x \to 0^+} \varphi(x) = -\frac{F\ a}{EI\sqrt{\alpha}}. \tag{31}$$

This relation also results in $c_3 = -Fa/(EI\sqrt{\alpha})$ for $-a \le x \le 0$. Thus, cross-sectional rotations of the upper arm can be defined over the entire domain as

$$\varphi(x) = \begin{cases} \frac{F}{EI}\left(\frac{x^2}{2} + a\,x - \frac{a}{\sqrt{\alpha}}\right) & \text{for } -a \le x \le 0, \\ -\frac{F\ a}{EI\ \sqrt{\alpha}} e^{-\sqrt{\alpha}x} & \text{for } x \ge 0. \end{cases} \tag{32}$$

2.3. The case of Euler-Bernoulli theory

Solutions for the case when Euler-Bernoulli beam theory is used to model the arms can be obtained as limit values of Timoshenko beam theory solutions when $\mu A_s \to \infty$. Because

$$\lim_{\mu A_s \to \infty} \alpha = \infty, \tag{33}$$

functions (15)–(18) will all return zero values for any $x > 0$. By taking into account the entire domain ($x \ge -a$) we can write

$$\sigma(x) = 0 \quad \text{for} \quad -a \le x < 0 \text{ and } x > 0, \tag{34}$$

$$\mathscr{T}(x) = \begin{cases} F & \text{for } -a \le x < 0, \\ 0 & \text{for } x > 0 \end{cases} \tag{35}$$

$$\mathscr{M}(x) = \begin{cases} F(x+a) & \text{for } -a \le x \le 0, \\ 0 & \text{for } x > 0 \end{cases} \tag{36}$$

$$\varphi(x) = \begin{cases} \frac{F}{EI}\left(\frac{x^2}{2} + a\,x\right) & \text{for } -a \le x \le 0, \\ 0 & \text{for } x \ge 0. \end{cases} \tag{37}$$

Note that, in order to obtain the equilibrium of transverse forces and moments around the crack tip, at the crack tip there must exist a concentrated force, F_0, pointing downwards and an anti-clockwise concentrated moment, M_0, defined as

$$F_0 = F, \quad \text{and} \quad M_0 = F\ a, \tag{38}$$

respectively. Such boundary conditions at the crack tip imply that the arms are clamped, which is additionally confirmed in Equation (37) giving $\varphi(0) = 0$. In this case, on the interface, the tensile-stress zone remains concentrated at the crack tip, while the compressive-stress zone also shrinks to a single point, again at the crack tip. Note that $\sigma(x)$ is not defined for $x = 0$ in (34), because of the stress singularity at the crack tip. Note also that, because $\varphi(x) = 0$ for $x > 0$, the arms are undeformed in front of the crack tip. Thus, we can conclude that Euler-Bernoulli beam theory indeed returns clamped conditions at the crack tip, meaning that in that case ESBT corresponds to SBT.

Remark 2.2. Additionally, in Appendix A.1, we extend the closed-form solution derived in in this section to the case of a DCB with prescribed rotations. ■

3. Enhanced simple beam theory (ESBT) and simple beam theory (SBT) expressions for G_c

Based on the solutions derived in the previous section, here we derive a novel formula for G_c based on the presented ESBT model. This formula can be considered as a general LEFM solution, from which two particular formulae available in the literature can be derived, for the cases of (i) Timoshenko beam theory with the arms clamped at the crack tip (SBT-T) and (ii) Euler-Bernoulli beam theory (SBT-E).

3.1. Enhanced simple beam theory (ESBT)

The crack mouth opening displacement, δ, can be computed assuming that the detached part of the DCB ($-a \le x \le 0$) acts like a Timoshenko cantilever beam with an initial rotation $\varphi(0) = -Fa/(EI\sqrt{\alpha})$, as defined in (31). Thus, using classic beam deflection formulae and assuming deflections of both arms we can write

$$\delta = 2[\delta_c - \varphi(0)\,a], \tag{39}$$

where

$$\delta_c = \frac{F\ a^3}{3\ EI} + \frac{F\ a}{\mu A_s}, \tag{40}$$

is the deflection of a shear-deformable (fully clamped) cantilever beam. Finally, we obtain

$$\delta = 2\left(\frac{F\ a^3}{3\ EI} + \frac{F\ a(1 + a\ \sqrt{\alpha})}{\mu A_s}\right). \tag{41}$$

The critical energy release rate, G_c, has the general expression

$$\dot{a} > 0 \Rightarrow G_c = -\frac{1}{b}\frac{\partial \Pi}{\partial a}, \tag{42}$$

where the dot represents the derivative with respect to time (i.e. $\dot{a} > 0$ means that the crack is propagating) and Π is the total potential energy. For this case, we can consider one of the two equivalent cases of prescribed displacement or prescribed force. Although the former is chosen in a real experiment, the latter is more convenient for the analytical derivation and gives

$$\Pi = -\frac{F\,\delta}{2} \tag{43}$$

Therefore we have

$$G_c = \frac{F}{2b}\frac{\mathrm{d}\delta}{\mathrm{d}a}, \tag{44}$$

from which, using (41), we can obtain

$$G_c = \frac{F^2}{b}\left(\frac{a^2}{EI} + \frac{1 + 2a\sqrt{\alpha}}{\mu A_s}\right) \quad \text{for ESBT.} \tag{45}$$

This novel formula, so far as authors are aware, has not been presented in the literature as yet. Because it is based on the ESBT model, which removes the SBT assumptions so far used by other authors, it is also the only correct formula for G_c for the LEFM limit case and Timoshenko beam theory. Expression (45) can be also written as

$$G_c = \frac{(F\,a)^2}{b\,EI}\left(1 + \frac{1}{a\sqrt{\alpha}}\right)^2 \quad \text{for ESBT.} \tag{46}$$

Remark 3.1. Expression (46) is similar to those reported by Suo et al. [13] and Bao et al. [14], where instead of the coefficient $1/(a\sqrt{\alpha})$, the product $Y_1(\rho)\lambda^{-1/4}h/a$ is used. Parameters λ and ρ in their expressions are functions of material constants for the plane-stress orthotropic case (E_1, E_2, μ_{12} and ν_{12} or ν_{21}), whereas $Y_1(\rho)$ is the quadratic [13] or cubic [14] fit of the finite element solutions for the plane elasticity problem. This means that $Y_1(\rho)$ accounts for some additional effects (through-the-thickness compressibility of the arms, in-plane warping of the arms' cross-sections etc.), that cannot be captured using beam models. Therefore, it can be expected that expressions for G_c from Refs. [13,14] describe better the real behaviour of a DCB specimen, than expression (46). On the other hand, although the method proposed in Refs. [13,14] is effectively a way of correcting the LEFM solution by taking into account the deformation in front of the crack tip, such correction does not take into account the deformation and damage of the interface, unlike other more widely used methods, e.g. CBT and ECM [3]. More importantly, the main problem in the practical use of this method in real-life applications is that it requires the measurement of the crack length. A better alternative, as presented in Refs. [6,7,9,15] and in the present paper, is to use data-reduction schemes that do not require the measurement of the crack length and are based on the concept of equivalent crack length. It is also worth mentioning that formulae for G_c used in Refs. [13,14] are based on the work of Gillis and Gilman [16], which was later extended by Wiederhorn et al. [17] and Srawley and Gross [18]. ■

3.2. Timoshenko beam theory with arms clamped at the crack tip (SBT-T)

If we assume that the arms of the DCB are clamped at the crack tip we have $\varphi(0) = 0$, which means that, according to (39), we have

$$\delta = 2\delta_c = 2\left(\frac{F\,a^3}{3\,EI} + \frac{F\,a}{\mu A_s}\right). \tag{47}$$

Thus, from (44) we obtain

$$G_c = \frac{F^2}{b}\left(\frac{a^2}{EI} + \frac{1}{\mu A_s}\right) \quad \text{for SBT} - \text{T.} \tag{48}$$

Note that ESBT formula for G_c (45), compared to SBT-T formula for G_c (48), has an additional term which takes into account the rotation at the crack tip.

Remark 3.2. Expression (48) for G_c is equivalent to that proposed by Ripling et al. [1] used in ASTM D3433-99(2012) [2] and also in BS ISO 25217:2009 [3] in the SBT data reduction scheme. However, in that formula for G_c it is assumed that the material of the arms is isotropic with $\nu = 1/3$ and the value of shear correction coefficient is $k_s = 2/3$.

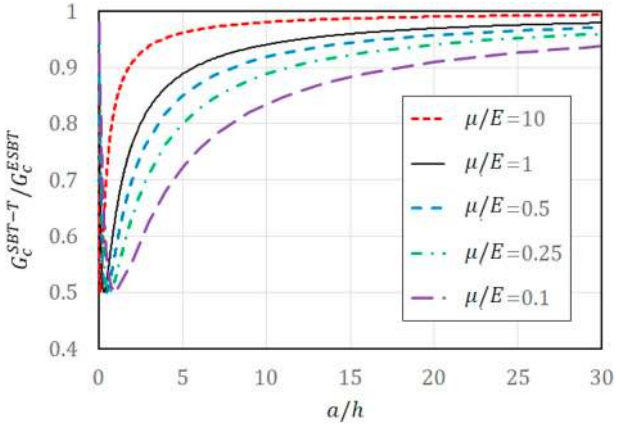

Fig. 3. Ratio G_c^{SBT-T}/G_c^{ESBT} (expressions (48) and (45)) with respect to the normalised crack length (a/h) for different values of μ/E.

Because in our approach values of E, μ and k_s can be independently assigned (although for a rectangular cross-section we exclusively use $k_s = 5/6$), Equation (48) can be considered as a general form of the SBT formula. Moreover, de Moura et al. [7] use formula (48) in their 'compliance based beam method' (CBBM). ■

Remark 3.3. Expressions (45) and (48) can be also considered as data reduction schemes, where, assuming that geometry and material of the arms are known, a and F are the only measured quantities. Therefore, for the same values of b, EI, μA_s, F and a, we can derive the ratio between expressions (48) and (45) as

$$\frac{G_c^{SBT-T}}{G_c^{ESBT}} = 1 - \frac{2\,a\sqrt{\alpha}}{(a\sqrt{\alpha} + 1)^2}, \tag{49}$$

where for a rectangular cross-section

$$a\sqrt{\alpha} = \sqrt{10}\,\frac{a}{h}\sqrt{\frac{\mu}{E}}. \tag{50}$$

Fig. 3 shows the values of the ratio (49) with respect to the normalised crack length (a/h) for different values of μ/E. It can be noted that the more shear deformable the arms (lower values of μ/E and a/h), the bigger the difference between G_c^{SBT-T} and G_c^{ESBT}. On the contrary, if shear stiffness of the arms is increased (which in the limit case leads to Euler-Bernoulli beam theory), the value of ratio (49) approaches 1. This confirms that in the limit case of Euler-Bernoulli beam theory ESBT corresponds to SBT-E. It can be also noted that, independently on the value of μ/E, the ratio (49) cannot be less than 0.5, i.e. G_c^{SBT-T} cannot be less than 50% of G_c^{ESBT}. This result can be easily confirmed analytically, where the minimum of ratio (49) is obtained for $a/h = \sqrt{E/(10\mu)}$. ■

3.3. Euler-Bernoulli beam theory (SBT-E)

In Section 2.3 we have shown that for the limit case of Euler-Bernoulli beam theory the arms are clamped at the crack tip so that, according to (37), $\varphi(0) = 0$. Thus, by letting $\mu A_s \to \infty$, Equation (39) results in

$$\delta = \frac{2\,F\,a^3}{3\,EI}. \tag{51}$$

Equation (44) in this case gives us

$$G_c = \frac{F^2\,a^2}{b\,EI} \quad \text{for SBT} - \text{E.} \tag{52}$$

This is a well-known LEFM formula for G_c [19], which is also the basis for some more sophisticated data reduction schemes, such as CBT and ECM from BS ISO 25217:2009 [3].

4. Data reduction schemes that do not require the crack-length measurement

The expressions for G_c derived in the previous section for cases of ESBT, SBT-T and SBT-E can be also considered as data reduction schemes. This means that, for known material and geometrical properties of the specimen (b, EI and μA_s), expressions (45), (48) and (52) could be used to compute G_c from experimental data consisting of the crack length, a, and the applied force, F.

However, optical determination of the position of the crack tip is difficult, time consuming and a significant source of inaccuracy in the results. This was a motivation for many authors [7,8,15,20] to propose approaches for computing G_c that do not require the measurement of the crack length. Because the cross-head opening displacement, δ, can be accurately measured directly from the testing machine, the idea is to use this parameter instead of a in formulae for G_c.

4.1. Concept of 'equivalent crack length'

For the three cases from Section 3 (ESBT, SBT-T and SBT-E), using Equations (41), (47) and (51), it is possible to express a in terms of F and δ, i.e. $a = a(F, \delta)$, and replace it in the corresponding expressions (45), (48) and (52) for G_c. This has been the approach used in Refs. [7–9,15] for the SBT-T and SBT-E cases, which is here extended to the ESBT case.

However, the implications of using simplified beam theory models was not recognised in the above-mentioned earlier work by other authors. This is because, as noted in Ref. [6], the crack-mouth opening displacement, δ, computed from (41), (47) or (51), using the real measured values of the applied force, F, and of the crack length, a, is different from the actual (measured) value of δ. This would happen also in an ideal case with no measurement errors and the material and geometrical properties known with no uncertainty. Focussing on the cases contemplated by the test standards considered in this work, i.e. adhesive joints or composite delamination, there will normally be a difference between the measured displacement and that given by (41), due to aspects including 3D effects, through-the-thickness deformation of the arms, geometrical non-linearities, possible rate-dependent response, interface compliance, a finite-size cohesive zone, possibly also due to fibre-bridging.

For this reason, using the measured values of F and δ, for each of the theories considered here, the following expressions can be written:

$$\delta = 2\left(\frac{F\, a_{eq}^3}{3\, EI} + \frac{F\, a_{eq}(1 + a_{eq}\sqrt{\alpha})}{\mu A_s}\right), \text{ for ESBT} \tag{53}$$

$$\delta = 2\left(\frac{F\, a_{eq.T}^3}{3\, EI} + \frac{F\, a_{eq.T}}{\mu A_s}\right) \text{for SBT} - \text{T}, \tag{54}$$

$$\delta = \frac{2\, F\, a_{eq.E}^3}{3\, EI} \text{for SBT} - \text{E}, \tag{55}$$

where a_{eq}, $a_{eq.T}$ and $a_{eq.E}$ are the equivalent crack lengths for ESBT, SBT-T and SBT-E. The word 'equivalent' is used because they are the values of the crack lengths that make the relevant expressions for δ valid when the measured values of F and δ are used.

4.2. Data-reduction schemes based on the concept of 'equivalent crack length'

Although the concept of 'equivalent crack length' has been discussed by De Moura et al. [7], the difference between the actual (a) and the equivalent (a_{eq}) crack length was not rigorously taken into account in the derivation of the expression for G_c. The actual crack length, a, in the expression for G_c equivalent to (48) was simply substituted by the equivalent one, a_{eq}, which was then expressed in terms of F and δ using relation (54). However, this procedure is not rigorous because, as explained in Section 4.1, $a \neq a_{eq}$. A similar approach was used in Refs. [8,9,15] for the case of Euler-Bernoulli beam theory, where a in expression for G_c (52) was expressed in terms of F and δ using (51). By doing so, it is assumed that the actual (measured) values of F, δ and a satisfy relation (51), which is not correct.

Therefore, the concept of equivalent crack length must be correctly implemented in order to obtain valid expressions for G_c. First of all, in Equation (44), δ must be expressed using expressions (53)–(55), i.e. $\delta = \delta(F, a_{eq})$ must be used instead of $\delta = \delta(F, a)$. It is extremely important to note that the critical energy release rate is obtained by taking the derivative with respect to the actual crack length, and not the equivalent one (see Equation (42)). As a result, in Equation (44), we need to write:

$$\frac{\mathrm{d}\delta}{\mathrm{d}a} = \frac{\mathrm{d}\delta}{\mathrm{d}a_{eq}}\left(\frac{\mathrm{d}a_{eq}}{\mathrm{d}a}\right), \quad \text{or} \quad \frac{\mathrm{d}\delta}{\mathrm{d}a} = \frac{\mathrm{d}\delta}{\mathrm{d}a_{eq.T}}\left(\frac{\mathrm{d}a_{eq.T}}{\mathrm{d}a}\right), \quad \text{or} \quad \frac{\mathrm{d}\delta}{\mathrm{d}a} = \frac{\mathrm{d}\delta}{\mathrm{d}a_{eq.E}}\left(\frac{\mathrm{d}a_{eq.E}}{\mathrm{d}a}\right), \tag{56}$$

depending on which theory (EBST, SBT-T or SBT-E) we are using in the model.

Thus, considering (56), substituting (53)–(55) in (44) gives

$$G_c = G_c^* \frac{\mathrm{d}a_{eq}}{\mathrm{d}a} \text{for ESBT}, \tag{57}$$

$$G_c = G_c^T \frac{\mathrm{d}a_{eq.T}}{\mathrm{d}a} \text{for SBT} - \text{T}, \tag{58}$$

$$G_c = G_c^E \frac{\mathrm{d}a_{eq.E}}{\mathrm{d}a} \text{for SBT} - \text{E}, \tag{59}$$

where

$$G_c^* = \frac{F^2}{b}\left(\frac{a_{eq}^2}{EI} + \frac{1 + 2\, a_{eq}\sqrt{\alpha}}{\mu A_s}\right), \tag{60}$$

$$G_c^T = \frac{F^2}{b}\left(\frac{a_{eq.T}^2}{EI} + \frac{1}{\mu A_s}\right), \tag{61}$$

$$G_c^E = \frac{F^2\, a_{eq.E}^2}{b\, EI}. \tag{62}$$

Note that using the same measured data (a, F and δ), formulae (57)–(59) return the same value of G_c, independently on the beam theory used or conditions assumed at the crack tip. The before-mentioned approaches from the literature [7–9,15], in fact, give only the values of G_c^T and G_c^E, but not the actual value of G_c. The exact value of G_c can be computed only if we can compute the derivatives $\mathrm{d}a_{eq}/\mathrm{d}a$, $\mathrm{d}a_{eq.T}/\mathrm{d}a$ and $\mathrm{d}a_{eq.E}/\mathrm{d}a$. This would, however, require the knowledge (i.e. measurement) of the actual crack length, a.

In Ref. [6] we used an FE model with a quasi brittle interface to produce virtual experimental data (values of F, δ and a). We showed that, even for cases of extremely ductile interfaces in the virtual experiments, the values of the derivatives $\mathrm{d}a_{eq.T}/\mathrm{d}a$ and $\mathrm{d}a_{eq.E}/\mathrm{d}a$ are very close to 1. Therefore, formulae for G_c^T and G_c^E can be considered as very accurate approximations for G_c in a wide range of cases of practical interest, such as those studied in Ref. [6]. Moreover, because they do not require the measurement of the crack length, they can be also considered as reliable and practical data reduction schemes. It is reasonable to expect that similar and even higher accuracy in the determination of G_c can be obtained using the ESBT-based value G_c^* because ESBT theory removes the simplifying assumptions made in SBT-T and SBT-E-based models.

Based on the discussion from the previous paragraph, we will introduce three data-reduction schemes, namely ESBT, SBT-T and SBT-E, that do not require the crack-length measurement and are based on

expressions (60), (61) and (62), respectively. At this point it is extremely important to distinguish these data-reduction-scheme formulae from the exact formulae for G_c given in (45), (48) and (52) for each particular case. Unlike the exact formulae for G_c, the mentioned data-reduction schemes to not require the crack-length measurement. In Section 5 we will show that ESBT is not only the most accurate data reduction scheme that does not require the crack-length measurement, but is also more accurate than the most accurate data-reduction scheme from the standards, which happens to be CBT [3]. Note also that data reduction schemes equivalent to SBT-T and SBT-E have been proposed in Refs. [7–9,15].

Nevertheless, to make our EBST, SBT-T and SBT-E data-reduction schemes complete, we need to compute a_{eq}, $a_{eq.T}$ and $a_{eq.E}$ from the measured values of F and δ. From expressions (53)–(55) it is obvious that this requires solving cubic equations for a_{eq}, $a_{eq.T}$ and $a_{eq.E}$.

The closed-form solution of cubic equation (53) for a_{eq} reads

$$a_{eq} = \sqrt[3]{\left(\frac{1}{\sqrt{\alpha}}\right)^3 + a_{eq.E}^3} - \frac{1}{\sqrt{\alpha}}, \quad \text{for ESBT,} \tag{63}$$

where

$$a_{eq.E} = \sqrt[3]{\frac{3\,EI\,\delta}{2\,F}}, \quad \text{for SBT} - \text{E,} \tag{64}$$

is the solution of Equation (55) for a for the SBT-E case.

The closed-form solution of cubic equation (54) for $a_{eq.T}$ reads

$$a_{eq.T} = \sqrt[3]{\chi} - \frac{1}{\alpha\sqrt[3]{\chi}}, \quad \text{for SBT} - \text{T,} \tag{65}$$

where

$$\chi = \sqrt{\frac{1}{\alpha^3} + \left(\frac{a_{eq.E}^3}{2}\right)^2} + \frac{a_{eq.E}^3}{2}. \tag{66}$$

Note that a_{eq}, $a_{eq.T}$ and $a_{eq.E}$ given here are the only real roots of (53), (54) and (55), respectively. See e.g. Ref. [21] for the detail on the analytical solution of a cubic equation. In the CBBM approach proposed by De Moura et al. [7], which is based on SBT-T, the related cubic equation is solved numerically. Solving Equation (55) for $a_{eq.E}$ provides the solution given in (64) and denoted as $a_{eq.E}$. This result was used in Refs. [8,9,15] to eliminate a from expression (52) for G_c.

Remark 4.1. In Appendix A.2, based on the solutions derived in Appendix A.1, we obtain a well-known formula for G_c [22] for DCB with prescribed rotations, which does not require the measurement of the crack length. Moreover, we show that in that case $da_{eq}/da = da_{eq.T}/da = da_{eq.E}/da = 1$ and the crack propagation is steady state. Although the derived formula (A.11) for G_c could be used as the most accurate data-reduction scheme, prescribing equal and opposite rotations on the arms requires sophisticated experimental rigs [23,24] which makes the testing procedure less practical. In Section 5 we will show that the errors in computing Ω or G_c using expressions for G_c^*, G_c^T and G_c^E for the case of DCB with prescribed displacement are very small and effectively negligible for brittle interfaces (especially when ESBT model is used). Thus, because prescribing displacement is also much more practical than prescribing rotations, from an engineering point of view it is recommended that future standards continue to be based on the DCB test with prescribed displacement. ■

5. Numerical assessment of accuracy of the data-reduction schemes

In this section we will assess the accuracy of the data reduction schemes used in BS ISO 25217:2009 [3] and the three data reduction schemes presented in Section 4 based on the equivalent-crack-length approach.

Table 1
Overview of the data reduction schemes used in the present comparison.

Label	Fracture toughness (G_c)	Measured quantities	Computed quantities
SBT	$\frac{4F^2}{Eb^2}\left(\frac{3a^2}{h^3}+\frac{1}{h}\right)$	a, F	–
CBT	$\frac{3F\delta}{2b(a+a_c)}$	a, F, δ	a_c (requires linear fit of the measured data)
ECM	$\frac{nF\delta}{2ba}$	a, F, δ	n (requires linear fit of the measured data)
ESBT	$\frac{F^2}{b}\left(\frac{a_{eq}^2}{EI}+\frac{1+2a_{eq}\sqrt{\alpha}}{\mu A_s}\right)$	F, δ	$a_{eq} = \sqrt[3]{\left(\frac{1}{\sqrt{\alpha}}\right)^3 + a_{eq.E}^3} - \frac{1}{\sqrt{\alpha}}$, where $\alpha = \frac{\mu A_s}{EI}$
SBT-T	$\frac{F^2}{b}\left[\frac{a_{eq.T}^2}{EI}+\frac{1}{\mu A_s}\right]$	F, δ	$a_{eq.T} = \sqrt[3]{\chi} - \frac{1}{\alpha\sqrt[3]{\chi}}$, where $\chi = \sqrt{\frac{1}{\alpha^3} + \frac{(a_{eq}^E)^6}{4}} + \frac{(a_{eq}^E)^3}{2}$
SBT-E	$\frac{F^2 a_{eq.E}^2}{b\,EI}$	F, δ	$a_{eq.E} = \sqrt[3]{\frac{3\,EI\,\delta}{2F}}$

There are three data reduction schemes in BS ISO 25217:2009 [3], namely 'simple beam theory' (SBT), 'corrected beam theory' (CBT) and 'enhanced compliance method' (ECM). The expressions for G_c for each of these methods are given in Table 1. In Remark 3.2 we have already mentioned that the SBT formula for G_c from Ref. [3] is a specific case of formula (48). The term a_c in the CBT expression for G_c represents the crack length correction, which is obtained graphically from the $\log a - \log C^{1/3}$ plot, where $C = \delta/F$ is the measured compliance. Factor n in the ECM expression for G_c is the slope of the linear fit of the $\log a - \log C$ data and is also obtained graphically. Note that all methods from the current version of the British Standard require the measurement of the crack length a (as indicated in Table 1). More details about these methods can be found in Ref. [3].

The data-reduction schemes presented in Section 4 based on the equivalent-crack-length concept, ESBT, SBT-T and SBT-E, are also summarised in Table 1. For ESBT we use Equation (60) for G_c^* and expression (63) to compute the equivalent crack length. We use Equation (61) to compute G_c^T, whereas the equivalent crack length for SBT-T is computed using (65). For SBT-E we use (62) for G_c^E and (64) for the equivalent crack length.

5.1. Virtual experiments

5.1.1. Motivation

To compare the accuracy of different data reduction schemes we present three different examples, all based on experimental tests reported in the literature, but instead of using the actual experimental data, we create 'virtual' experimental data. This is done by fitting the actual experimental load-displacement ($F-\delta$) curves using a finite-element (FE) model. Assuming that the interface properties of the model are constant along the interface, we use $F-\delta$ data from our virtual experiments (which is extremely close to the actual experimental $F-\delta$ data) to compute G_c using different data reduction schemes presented in Table 1. The virtual experiments also give us the actual crack length, a, which is necessary to compute G_c using data reduction schemes from BS ISO 25217:2009 [3]. Moreover, knowing the actual values of a allows us to compute the derivatives da_{eq}/da, $da_{eq.T}/da$ and $da_{eq.E}/da$, which are necessary to compute the correct value of G_c (see Equations (57–59)). These derivatives are computed numerically using a 5-point central difference formula reported in Ref. [6].

5.1.2. Beam model vs. 2D plane-stress model

In the present work we use two types of FE models for virtual experiments: (i) beam model and (ii) 2D plane-stress model. Because it is assumed that DCB is symmetric with respect to the mid-plane of the

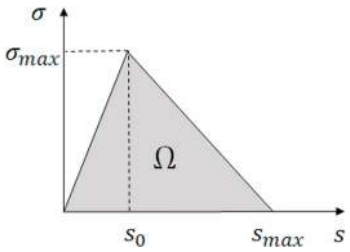

Fig. 4. A standard bi-linear traction-separation law of a CZM.

interface, only one arm is modelled in both cases.

Beam model, originally proposed in Ref. [25], consists of Timoshenko beam elements and interface elements with an embedded bi-linear cohesive-zone model (CZM), as the one shown in Fig. 4. The area under the bi-linear traction-separation law ($\sigma - s$) is given by

$$\Omega = \frac{\sigma_{max}\, s_{max}}{2}, \tag{67}$$

where σ_{max} is the maximum allowed value of the contact traction σ and s_{max} is the maximum value of the relative displacement at the interface s before the interface is fully damaged. The initial stiffness of the interface is defined by $k = \sigma_{max}/s_0$, where s_0 is the maximum relative displacement at the interface before the softening of the interface starts to taking place.

Although neither of the models used for virtual experiments is able to fully account for 3D effects, they can be partially accounted for by determining an equivalent Young's modulus. Unlike the 2D plane-stress model, the beam model cannot capture the influence of the through-the-thickness deformation in the arms. In Ref. [5], it was shown that the differences between the Euler-Bernoulli beam model (closed-form) solutions and 2D plane-stress model FE analysis solutions are not negligible. On the other hand, in Ref. [25] it was demonstrated that Timoshenko beam model can be used to substitute more complex 2D models without any significant loss of accuracy. This is confirmed also in the present work, as shown in Figs. 5–7.

Because in our virtual experiments the input value of Ω is known in advance and the values of the actual crack length, a, can be easily obtained, we assess the accuracy of data reduction schemes from Table 1 based on how close they predict the value of Ω. The comparison of different data reduction schemes is given in terms of normalised fracture resistance, which is defined as G_c/Ω, where G_c is defined differently for each data reduction scheme presented in Table 1.

Even though 2D plane-stress model provides a more accurate modelling of the problem, in this work we present the results using the Timoshenko beam model because for the LEFM limit case ($\sigma_{max} \to \infty$ and $s_{max} \to 0$) this model corresponds exactly to ESBT model (see Section 2). Therefore, any differences between G_c computed using the ESBT data-reduction scheme and Ω in the Timoshenko beam FE model can be attributed only to different models of the interface (LEFM vs. cohesive zone of finite size). Moreover, we can asses the inaccuracy related to the deformation of the beam in front of the crack tip (accounted for in our ESBT, but neglected in the SBT or approximately taken into account in the ECM and CBT [3]) in a clear way.

Remark 5.1. In Ref. [6] we showed that in general G_c is not equal to the work of separation (the area under the traction-separation law), Ω, of the CZM. Their difference is given by the derivative, with respect to the crack length, of the energy dissipated ahead of the crack tip per unit of specimen width. For a steady-state crack propagation, in which that energy remains constant as the crack tip advances, this derivative vanishes and $\Omega = G_c$. The virtual experiments presented in Ref. [6] showed that for a DCB with prescribed displacement and constant properties along the interface, the difference between Ω and G_c is negligible for brittle interfaces and very small for ductile interfaces. Crack propagation for a DCB with prescribed rotations is steady-state even if the interface is quasi-brittle (also shown in Ref. [6]). The difference between Ω and G_c is greater, though still very limited, for the cases where a rising R-curve (variation of properties along the interface) is modelled [6]. Furthermore, in Ref. [6] we also show that the proof that the critical value of the J integral, J_c, is equal to the nonlinear energy release rate is not valid for a non-homogeneous material. Nevertheless, in our virtual experiments $J_c = \Omega$ because Ω, as well as the other CZM parameters, are constant along the interface. ■

5.1.3. Modelling the real experiments

By fitting the real experimental $F - \delta$ curves, the maximum contact traction, σ_{max} and the maximum relative displacement at the interface before failure, s_{max}, for the CZM were obtained (see Fig. 4). In our numerical simulations we fix $s_0 = 0.01\, s_{max}$.

The fist example is a CFRP DCB with Hysol® 9309 adhesive reported by Blackman at al. [26], the second one is a DCB made of aluminium adherends and bonded with the epoxy adhesive Hysol® 9466 reported by Alfano et al. [15], and the third one, reported by Lopes et al. [20], is a DCB made of steel adherends bonded with the epoxy adhesive Sikaforce® 7752. All the relevant data used in virtual experiments is presented in Table 2. These examples cover a wide range of adhesive behaviours, from extremely brittle (experiment 1), to extremely ductile (experiment 3).

Beam FE simulations have been performed using our own code in Fortran, whereas 2D simulations have been performed in Abaqus software. 2200, 2000 and 3000 2-node Timoshenko beam FEs have been used to model Experiments 1, 2 and 3, respectively, whereas for the 2D model, meshes of 1294 × 7, 400 × 30 and 600 × 25 fully-integrated 4-node plane-stress solid rectangular elements (named CPS4 in Abaqus)

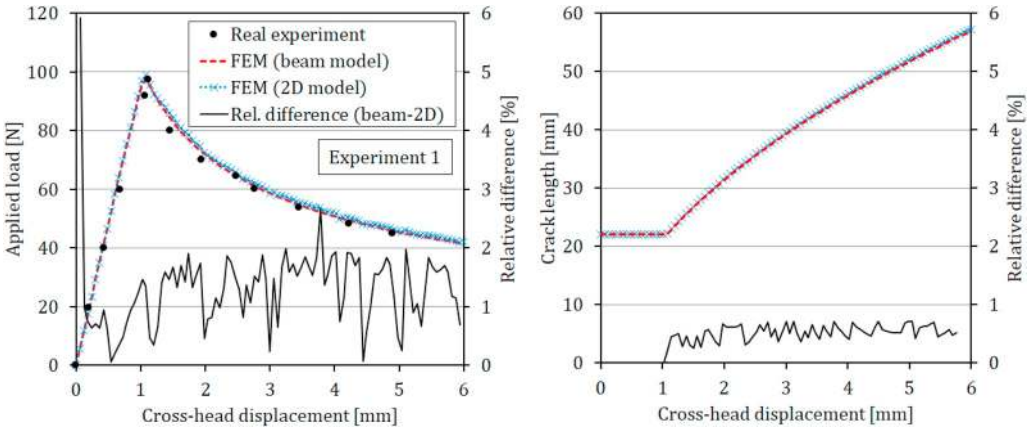

Fig. 5. Experiment 1 [27] - A comparison between beam and 2D plane-stress finite elements: (a) $F - \delta$ curve and (b) $a - \delta$ curve.

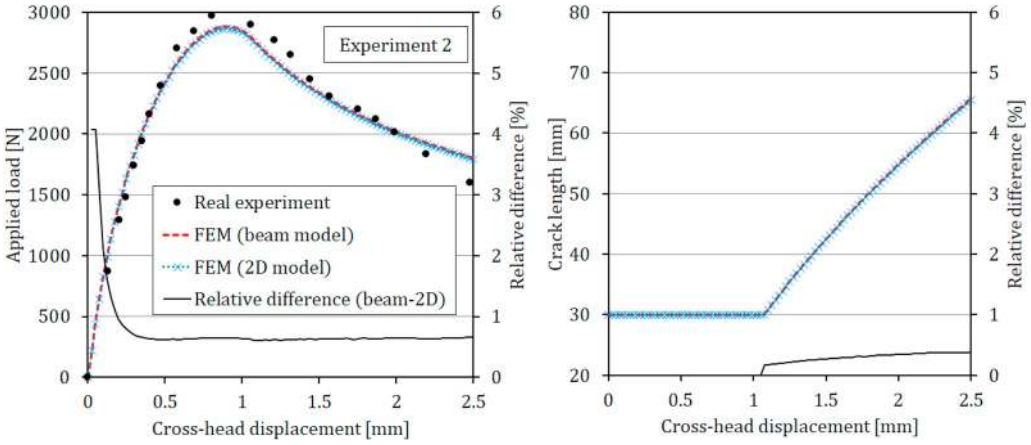

Fig. 6. Experiment 2 [15] - A comparison between beam and 2D plane-stress finite elements: (a) $F-\delta$ curve and (b) $a-\delta$ curve.

have been used. For both models, 4-node interface elements (named COH2D4 in Abaqus) of the same length as the elements used to model the arms have been used at the interface. Besides using the quantities reported in Table 2, CFRP from Experiment 1 has been modelled using $E_y = 8$ GPa and $\nu_{xy} = 0.34$ in the 2D model, where y is the vertical (transversal) direction. For the other two Experiments no data other than that reported in Table 2 has been necessary.

In Figs. 5–7, a comparison between beam and 2D plane-stress FE models is given in terms of F, δ and a for each experiment. It can be noted that the models agree extremely well and that their differences for the examined cases are negligible. For Experiment 1, the numerical noise in the relative difference is more pronounced, but the average values are still very low ($< 2\%$ for F and $< 1\%$ for a). These results confirm that Timoshenko beam model can be used instead of conventional 2D models without any significant loss of accuracy to model crack propagation in different types of DCB specimens.

Moreover, the beam FE model is computationally more efficient and robust than the compared 2D model. Displacement control has been used for for both models. Values of the displacement increment were 0.06, 0.025 and 0.1 mm for Experiments 1, 2 and 3, respectively. Using the beam model, 1 increment cut for Experiment 1 and 2 increment cuts for Experiment 3 were necessary to reach the desired value of the maximum displacement. For Experiment 2, the maximum displacement has been reached without any increment cuts.

For the 2D model, obtaining the solution was less straight-forward. Except for Experiment 1, an incremental, quasi-static fully-implicit analysis with the same time increments as for the beam models has been used. Because of the difficulties of achieving convergence, for Experiment 1 an implicit-dynamic analysis, with an initial displacement increment of 0.025 mm and a variable time increment, has been used. The output was recorded every 0.025 increments of prescribed displacement. A quasi-Newton iterative solution procedure was used in each increments, with the stiffness matrix reformed every 3 iterations.

Table 2
Data used in the set of virtual experiments (* isotropic $\nu = 1/3$,** isotropic $\nu = 0.3$).

Experiment	L	h	b	a_0	E	μ	Ω	σ_{max}
	[mm]	[mm]	[mm]	[mm]	[GPa]	[GPa]	[N/mm]	[MPa]
1	110	1.55	24	22	137	4.0	0.257	50
2	200	15	25	30	65.7	25.3*	2.7	14
3	300	12.7	25	55	204	78.6**	4.5	15

5.2. Numerical results

For the first experiment [26], the results in Fig. 8(a) show that CBT is the most accurate data reduction scheme from the British Standard [3] because it gives an excellent estimation of Ω for any position of the crack. The main reason why SBT is less accurate is that, due to both the compliance of the interface and the deformation of the arms in front of the crack tip, the measured crack length does not correspond to the one assumed in the model. This issue is also present in CBT and ECM, but because these data reduction schemes use corrections based on the measured compliance, the final results for G_c are more accurate.

Next, in Fig. 8(b), we compare the CBT predictions to those provided by the data reduction schemes of Section 4, which do not require

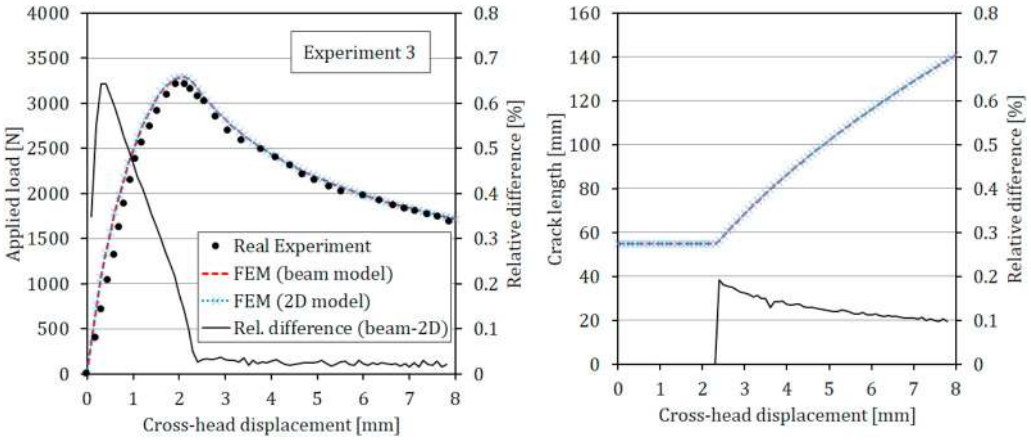

Fig. 7. Experiment 3 [20] - A comparison between beam and 2D plane-stress finite elements: (a) $F-\delta$ curve and (b) $a-\delta$ curve.

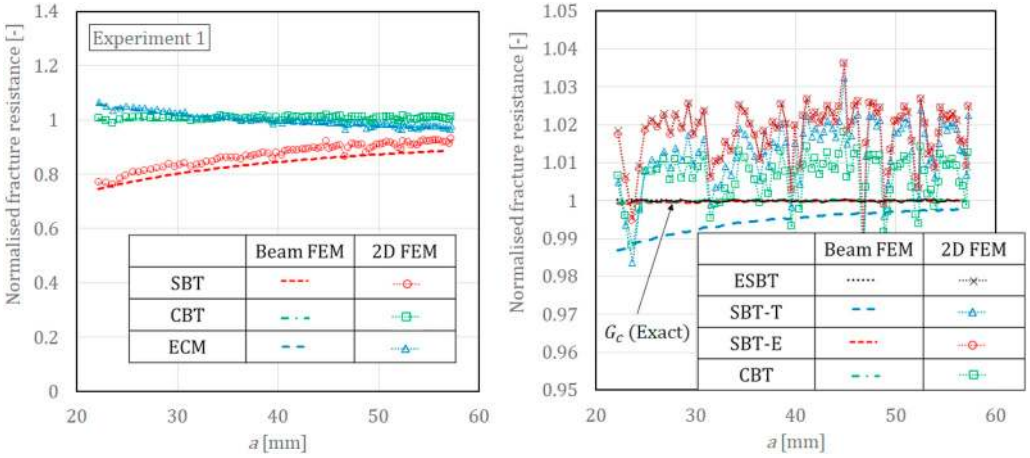

Fig. 8. Experiment 1 (CFRP with Hysol® 9309 [26]): a comparison between (a) the data reduction schemes from the British Standard [3] (SBT, CBT and ECM) and (b) the present data-reduction schemes that do not require measurement of the crack length (ESBT, SBT-T, SBT-E).

the measurement of the crack length (ESBT, SBT-T and SBT-E). It can be appreciated that all data-reduction schemes considered are extremely accurate, despite some numerical noise of the results from the 2D model. However, from the results from the beam model, we see that ESBT is the most accurate data reduction scheme, although the differences with respect to SBT-E and CBT are negligible. The adhesive in this example is very brittle (see Table 2) which makes its behaviour being extremely close to LEFM assumptions. Thus, this behaviour can be best captured using ESBT, where the equivalent crack length is extremely close to the actual one (which can be easily obtained from our virtual experiments). The assumption made in SBT-T (shear deformable arms clamped at the crack tip) results in lower values of the fracture resistance compared to the ones obtained in ESBT and SBT-E. It can also also seen that for this case, the accuracy of all data reduction schemes that do not require the measurement of the crack length (ESBT, SBT-T and SBT-E) is comparable to the accuracy of CBT (which does require measurement of the crack length).

Additionally, the exact value of G_c (computed from any of expressions (57)–(59)) normalised with respect to Ω is plotted in Fig. 8(b) and denoted as 'G_c (Exact)'. We can see that, for this case G_c is extremely close to Ω which means that the crack propagation is extremely close to being steady state. Moreover, because values of fracture resistance predicted using ESBT and SBT-E data-reduction schemes are extremely close to G_c, we can assume that $\mathrm{d}a_{eq}/\mathrm{d}a \approx 1$ and $\mathrm{d}a_{eq.E}/\mathrm{d}a \approx 1$. Only the result for the beam FE model is shown, because the result for 2D FE model contained a considerable amount of numerical noise. The same is done for Experiments 2 and 3, although there is less numerical noise.

The second experiment [15] features an adhesive with more pronounced ductility, which means that the actual behaviour of the DCB is not close to the LEFM assumptions. In Fig. 9(a) we can see that the results obtained using the data reduction schemes from the British Standard [3] are now less accurate. CBT, thanks to the crack length correction, is again the most accurate, whereas SBT is now extremely inaccurate. In Fig. 9(b) we can see that SBT-T again gives smaller values of the fracture resistance compared to ESBT and SBT-E, which, interestingly enough, in this case results in a better approximation of Ω. It can be noticed that in Fig. 9(b), the results of data-reduction schemes based on the concept of equivalent crack length obtained using the 2D model are slightly shifted with respect to the results obtained using the beam model.

The exact values of G_c are lower than Ω, which means that all the derivatives ($\mathrm{d}a_{eq}/\mathrm{d}a$, $\mathrm{d}a_{eq.T}/\mathrm{d}a$ and $\mathrm{d}a_{eq.E}/\mathrm{d}a$) are in this case less than 1. If we recall that the transversal displacements on the interface are not allowed in LEFM models, than we can conclude that in this virtual experiment these derivatives represent the influence of the interface compliance on the accuracy of a data-reduction scheme considered. Thus, the more ductile the interface, the less accurate a data-reduction scheme.

However, it is again important to note that the accuracy of the data reduction schemes that do not require the measurement of crack length (ESBT, SBT-T and SBT-E) is comparable to that of CBT predictions (or even higher for longer cracks). Note that, although the adhesive in this example is relatively ductile, the error in predicting the input value of Ω for all data reduction schemes presented in Fig. 9(b) is within ± 2%.

The adhesive in the third experiment [20] is extremely ductile. In Fig. 10(a) we see very similar behaviour as the one presented in Fig. 9(a) for the second experiment. The same applies to Fig. 10(b) which is very similar to Fig. 9(b). However, we can notice that for the third experiment all the data-reduction schemes provide predictions of Ω which are more accurate than for the second one, despite the adhesive in the third experiment being the most ductile one. The reason for this lies in the fact that the initial notch length, a_0, is considerably larger for the third experiment than for the second one. In fact, extending the curves in Fig. 10 to the left-hand side up to $a = 30$ mm would result in values that are less close to 1 than the ones presented in Fig. 9. Fig. 10(b) confirms that, although they are based on LEFM, all the data-reduction schemes considered in the present comparison are very accurate even for such a ductile adhesive, i.e. in the case when the damage-process zone has a length that is not small compared to specimen's dimensions. Results obtained using the beam model and the 2D model agree almost perfectly in this case.

5.3. Delamination of thick composite plates

In this section we will focus on the first experiment and see what would happen if the arms of the DCB were thicker. Besides the original thickness $h = 1.55$ mm, reported in Ref. [26] and Table 2, we will consider two additional cases in which the arms are twice and four times thicker. The results presented in Fig. 11 show that the ESBT data reduction scheme is the only one that can give an excellent accuracy in the case of delamination of relatively thick composite plates. In Fig. 11(a and b) we can observe that CBT and SBT-E are still highly accurate, whereas the accuracy of SBT-T is significantly lower than in the case with original depth of the arms (see Fig. 8(b)). Only the beam FE model has been used to obtain results for Fig. 11.

6. Conclusions

In this work we have presented a novel 'enhanced simple beam theory' (ESBT), in which a DCB is modelled using Timoshenko beam theory and LEFM assumptions. Unlike conventional simple beam theory (SBT), on which current standards are based, the rotations of the cross

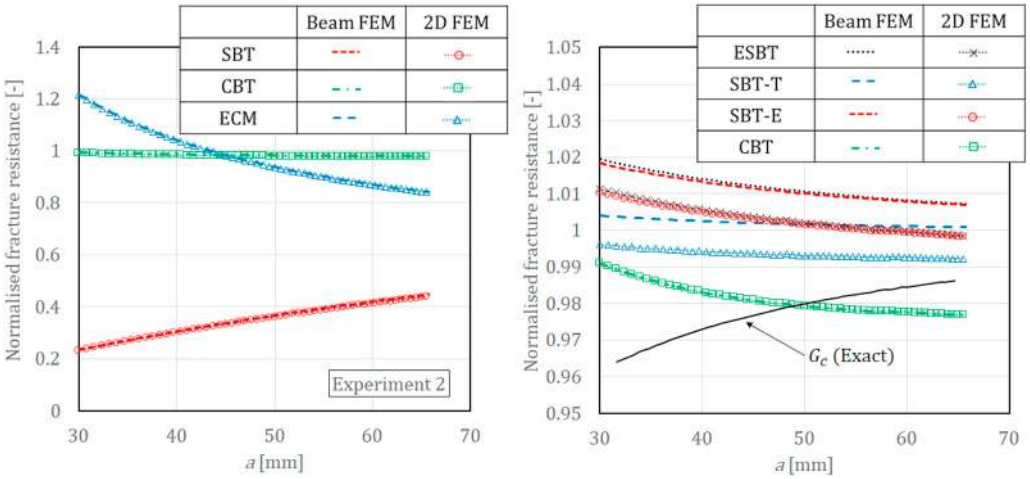

Fig. 9. Experiment 2 (aluminium Hysol® 9466 [15]): a comparison between (a) the data reduction schemes from the British Standard [3] (SBT, CBT and ECM) and (b) the present data-reduction schemes that do not require measurement of the crack length (ESBT, SBT-T, SBT-E).

sections in front of the crack tip are allowed in our formulation. The arms of the DCB rotate in front of the crack tip because of their shear-deformability. Consequently, when the arms are shear-rigid (which corresponds to Euler-Bernoulli beam theory) ESBT is equivalent to SBT and the clamped boundary conditions at the crack tip follow as a result.

Based on the ESBT solution, we derive a novel expression for the critical energy release rate, G_c, which takes into account the rotations of the arms at the crack tip. Furthermore, using the concept of 'equivalent crack length', we develop an ESBT-based data-reduction scheme for the determination of G_c that does not require measurement of the crack length. This is an important advantage with respect to the data reduction schemes from the standards [2,3], where such measurement is an essential part. We also compare the accuracy of ESBT data reduction scheme with that of two other data reduction schemes, obtained as particular cases of ESBT. These are SBT-T, where it is assumed that the arms are Timoshenko beams clamped at the crack tip (equivalent to CBBM [7]), and SBT-E, where the arms are assumed as Euler-Bernoulli beams (equivalent to what was proposed in Refs. [9,15]). Both SBT-T and SBT-E data reduction schemes use the equivalent-crack-length concept.

Our numerical results based on virtual experiments show that the data-reduction schemes that use the concept of equivalent crack length are as accurate as the most accurate data reduction scheme from the standards, which happens to be CBT from the British Standard [3]. ESBT, SBT-T and SBT-E can be all considered equally accurate for ductile adhesives, but for more brittle adhesives SBT-T is less accurate than the other two. In particular, if the adhesive is brittle and the arms have a more pronounced shear deformability, e.g. for the case of thick composite plates, ESBT is the most accurate data reduction scheme.

Our theoretical and numerical findings show that the data reduction schemes that use the concept of equivalent crack length should be seriously taken into account in future versions of the existing test standards. In this way, DCB tests could be performed without the time-consuming crack-length measurements, which would significantly simplify and speed up the procedure without any loss of accuracy in the characterisation of fracture resistance. However, a wide experimental study of available data reduction schemes, including the one presented in this paper, should be conducted to assess their accuracy for as many specimen geometries and materials as possible. As an alternative, virtual experiments with more sophisticated numerical models (which may include different traction-separation laws for CZM, rate-dependent CZMs, plasticity, 3D effects, fibre bridging etc.) can be used for further investigations.

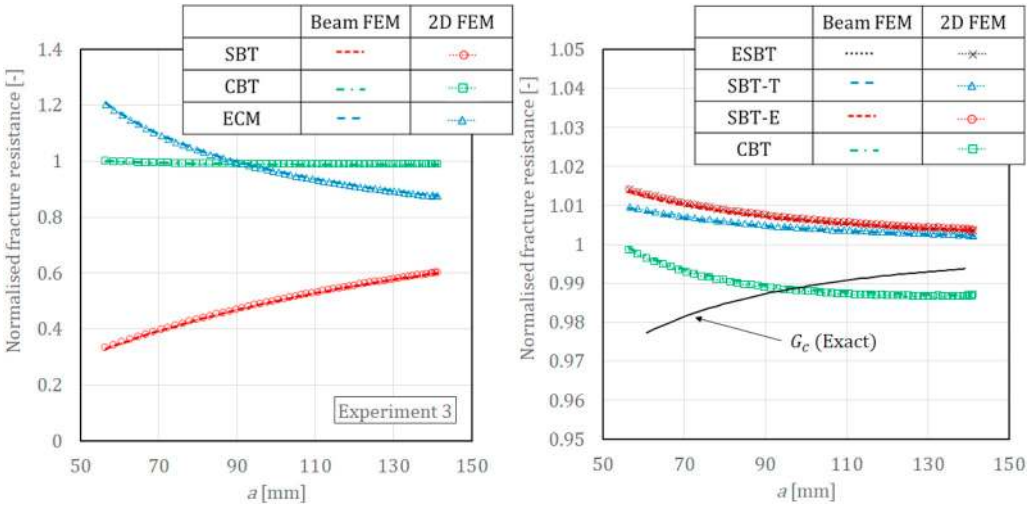

Fig. 10. Experiment 3 (steel with Sikaforce® 7752 [20]): a comparison between (a) the data reduction schemes from the British Standard [3] (SBT, CBT and ECM) and (b) the present data-reduction schemes that do not require the measurement of crack length (ESBT, SBT-T, SBT-E).

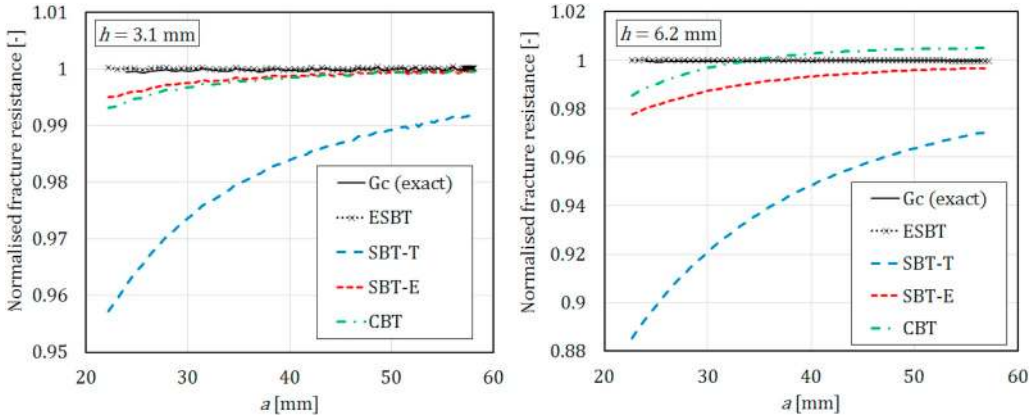

Fig. 11. Results for thick composite plates using ESBT, SBT-T, SBT-E and CBT data reduction schemes. Input data are as in Table 2 for the first experiment [26], but with an increased arm thickness equal to (a) 3.1 mm and (b) 6.2 mm.

Acknowledgments

This project has received funding from the European Union's Horizon 2020 research and innovation programme under the Marie Sklodowska-Curie grant agreement No 701032. The last author wishes to acknowledge the financial support of the Croatian Science Foundation (Research Projects IP-11-2013-1631 and IP-2016-06-4775).

Supplementary data

Supplementary data to this article can be found online at https://doi.org/10.1016/j.compositesb.2018.11.099.

Appendix A. LEFM solution for a Timoshenko DCB with prescribed rotations

Appendix A.1. Solution of the problem

If a DCB with prescribed rotations is considered, the same procedure presented in Section 2.2 can be followed. The main difference is that, in case of prescribed rotations, a concentrated moment, M, is applied at the left hand end of the upper arm, instead of the force, F. Thus, solution (4) is still valid and from boundary condition (11) again follows that $c_1 = 0$. However, the equilibrium of moments around the crack tip now reads

$$M - c_2 \int_0^{\infty} e^{-\sqrt{\alpha}x} x \, \mathrm{d}x = 0, \tag{A.1}$$

which after integrating by parts gives

$$c_2 = M\,\alpha. \tag{A.2}$$

If we compare this solution with equation (13) we can see that the moment Fa is simply substituted by M. The same thing occurs in Equations (14–18). Thus, by taking into account the entire domain ($x \geq -a$), we can define the functions of contact tractions at the interface, shear forces and bending moments in the upper arm as

$$\sigma(x) = \begin{cases} 0 & \text{for } -a \leq x < 0, \\ -\frac{M\,\alpha}{b} e^{-\sqrt{\alpha}x} & \text{for } x > 0, \end{cases} \tag{A.3}$$

$$\mathscr{T}(x) = \begin{cases} 0 & \text{for } -a \leq x < 0, \\ -M\,\sqrt{\alpha}\, e^{-\sqrt{\alpha}x} & \text{for } x > 0, \end{cases} \tag{A.4}$$

$$\mathscr{M}(x) = \begin{cases} M & \text{for } -a \leq x \leq 0, \\ M\, e^{-\sqrt{\alpha}x} & \text{for } x \geq 0, \end{cases} \tag{A.5}$$

Again, in order to satisfy the equilibrium of transversal forces, a concentrated reaction force $F_0 = M\sqrt{\alpha}$ pointed downwards must exist at the crack tip. Solving $\varphi(x) = \int \mathscr{M}(x)\mathrm{d}x/EI + c_3$ using Equation (A.5) results in $c_3 = 0$ for $x \geq 0$ and $\varphi(0) = c_3 = -M/(EI\sqrt{\alpha})$ for $-a \leq x \leq 0$, which finally gives

$$\varphi(x) = \begin{cases} \frac{M}{EI}\left(x - \frac{1}{\sqrt{\alpha}}\right) & \text{for } -a < x \leq 0, \\ -\frac{M}{EI\,\sqrt{\alpha}} e^{-\sqrt{\alpha}x} & \text{for } x \geq 0. \end{cases} \tag{A.6}$$

Appendix A.2. Expression for G_c

Using

$$\delta_c = \frac{M\ a^2}{2\ EI}, \tag{A.7}$$

from Equation (39) we can now obtain

$$\delta = \frac{M\ a^2}{EI} + \frac{2\ M\ a}{EI\ \sqrt{\alpha}}. \tag{A.8}$$

The potential energy is now computed as

$$\Pi = M\ \theta, \tag{A.9}$$

where θ is the prescribed rotation, i.e.

$$\theta = \varphi(-a) = -\frac{M}{EI}\left(a + \frac{1}{\sqrt{\alpha}}\right). \tag{A.10}$$

For prescribed rotations, using (A.9) and the definition for the critical energy release rate (42), we obtain

$$G_c = \frac{M^2}{b\ EI}. \tag{A.11}$$

Note that, although shear defromability of the arms has an influence on the cross-head displacement (A.8) and rotation (A.10), it has no influence on the formula for G_c. In fact, the same formula can be derived using the SBT assumptions both for Timoshenko [6] and Euler-Bernoulli beam theory [22,24] (as shown in the next subsection). Thus, for a DCB with prescribed rotations $G_c = G_c^* = G_c^T = G_c^E$ and $\mathrm{d}a_{eq}/\mathrm{d}a = \mathrm{d}a_{eq.T}/\mathrm{d}a = \mathrm{d}a_{eq.E}/\mathrm{d}a = 1$. Furthermore, because in a DCB with prescribed rotations crack propagates in a steady-state manner (as shown in Ref. [6]), for a quasi-brittle interface $\Omega = G_c = G_c^* = G_c^T = G_c^E$.

Appendix A.3. Euler-Bernoulli limit case

When Euler-Bernoulli beam theory is used to model the arms of a DCB with prescribed rotations (A.3) and (A.4) become $\sigma(x) = \mathscr{T}(x) = 0$, whereas Equations (A.5) and (A.6) now give

$$\mathscr{M}(x) = \begin{cases} M & \text{for } -a < x < 0, \\ 0 & \text{for } x > 0, \end{cases} \tag{A.12}$$

$$\varphi(x) = \begin{cases} \frac{M\ x}{EI} & \text{for } -a < x \le 0, \\ 0 & \text{for } x \ge 0. \end{cases} \tag{A.13}$$

Note that because the moments around the crack tip must be in equilibrium, a counter-clockwise concentrated moment reaction $M_0 = M$ must exist at the crack tip.

Because for Euler-Bernoulli beam theory $\alpha \to \infty$ from (A.10) we have

$$\theta = -\frac{M\ a}{EI}, \tag{A.14}$$

which from (A.9) again gives result (A.11) for G_c.

References

[1] Ripling EJ, Mostovoy S, Corten HT. Fracture mechanics: a tool for evaluating structural adhesives. J Adhes 1971;3(2):107–23.
[2] ASTM D3433-99(2012). Standard test method for fracture strength in cleavage of adhesives in bonded metal joints. ASTM International; 2012.
[3] BS ISO 25217. Adhesives - determination of the mode I adhesive fracture energy of structural adhesive joints using double cantilever beam and tapered double cantilever beam specimens. British Standard; 2009. 2009.
[4] ASTM D5528-13. Standard test method for mode I interlaminar fracture toughness of unidirectional fiber-reinforced polymer matrix composites. ASTM International; 2013.
[5] Biel A, Stigh U. Effects of constitutive parameters on the accuracy of measured fracture energy using the DCB-specimen. Eng Fract Mech 2008;75:2968–83.
[6] Škec L, Alfano G, Jelenić G. On G_c, J_c and the characterisation of the mode-I fracture resistance in delamination or adhesive debonding. Int J Solid Struct 2018;144–145:100–22.
[7] de Moura MFSF, Campilho RDSG, Gonçalves JPM. Crack equivalent concept applied to the fracture characterization of bonded joints under pure mode I loading. Compos Sci Technol 2008;68:2224–30.
[8] Tamuzs V, Tarasovs S, Vilks U. Delamination properties of translaminar-reinforced composites. Compos Sci Technol 2003;63:1423–31.
[9] Biel A, Stigh U. An analysis of the evaluation of the fracture energy using the DCB-specimen. Arch Mech 2007;59(4–5):311–27.
[10] Kanninen MF. An augmented double cantilever beam model for studying crack propagation and arrest. Int J Fract 1973;9(1):83–92.
[11] Williams JG. End corrections for orthotropic DCB specimens. Compos Sci Technol 1989;35:367–76.
[12] Shahani AR, Forqani M. Static and dynamic fracture mechanics analysis of a DCB specimen considering shear deformation effects. Int J Solid Struct 2004;41:3793–807.
[13] Suo Z, Bao G, Fan B, Wang TC. Orthotropy rescaling and implications for fracture in composites. Int J Solid Struct 1991;28(2):235–48.
[14] Bao G, Ho S, Suo Z, Fan B. The role of material orthotropy in fracture specimens for composites. Int J Solid Struct 1992;29(9):1105–16.
[15] Alfano M, Furgiuele F, Pagnotta L, Paulino G. Analysis of fracture in aluminum joints bonded with a bi-component epoxy adhesive. J Test Eval 2011;39(2):1–8.
[16] Gillis PP, Gilman JJ. Double-cantilever cleavage mode of crack propagation. J Appl Phys 1964;35(3):647–58.
[17] Wiederhorn SM, Shorb AM, Moses RL. Critical analysis of the theory of the double cantilever method of measuring fracture-surface energies. J Appl Phys 1968;39(3):1569–72.
[18] Srawley JE, Gross B. Stress intensity factors for crackline-loaded edge-crack specimens. NASA technical report; 1967. D-3820.
[19] Anderson TL. Fracture mechanics - fundamentals and applications. second ed. CRC Press; 1995.
[20] Lopes RM, Campilho RDSG, da Silva FJG, Faneco TMS. Comparative evaluation of the double-cantilever beam and tapered double-cantilever beam tests for estimation of the tensile fracture toughness of adhesive joints. Int J Adhesion Adhes 2016;67:103–11.
[21] Abramowitz M, Stegun IA. Handbook of mathematical functions. New York: Dover Publications, Inc.; 1972.
[22] Rice JR. A path independent integral and the approximate analysis of strain concentration by notches and cracks. J Appl Mech 1968;35:379–86.
[23] Freiman SW, Mulville DR, Mast PW. Crack propagation studies in brittle materials. J Mater Sci 1973;8:1527–33.
[24] Sørensen BF, Brethe P, Skov-Hansen P. Controlled crack growth in ceramics: the DCB specimen loaded with pure moments. J Eur Ceram Soc 1996;16:1021–5.
[25] Škec L, Jelenić G, Lustig N. Mixed-mode delamination in 2D layered beam finite elements. Int J Numer Methods Eng 2015;104:767–88.
[26] Blackman BRK, Hadavinia H, Kinloch AJ, Williams JG. The use of a cohesive zone model to study the fracture of fibre composites and adhesively-bonded joints. Int J Fract 2003;119:25–46.
[27] Blackman BRK, Kinloch AJ, Paraschi M, Teo WS. Measuring the mode I adhesive fracture energy, G_{IC}, of structural adhesive joints: the results of an international round-robin. Int J Adhesion Adhes 2003;23:293–305.